



Voltage-frequency dependence of the complex dielectric and electric modulus and the determination of the interface-state density distribution from the capacitance-frequency measurements of Al/p-Si/Al and Al/V₂O₅/p-Si/Al structures

Elvan Şenarslan^{1,2} · Mustafa Sağlam³

Received: 9 February 2024 / Accepted: 22 July 2024 / Published online: 21 August 2024
© The Author(s) 2024

Abstract

The energy distribution of the interface states (N_{ss}) and relaxation time (τ) are calculated from the capacitance-frequency ($C-f$) characteristics for Al/p-type Si/Al metal-semiconductor and Al/V₂O₅/p-type Si/Al metal–interfacial layer–semiconductor diodes with and without anodic surface passivation. The experimental results show that the density of the interface states and the relaxation times increase almost exponentially with the bias from the top of the valence band to the center of the gap for each diode produced. At the same time, using the $C-f$ characteristics, the dielectric properties such as the dielectric constant (ϵ'), dielectric loss (ϵ''), dielectric loss tangent ($\tan\delta$), real and imaginary portions of the electric modulus (M' and M'') and ac electrical conductivity (σ_{ac}) are investigated in this study. The analysis was performed at room temperature, in the frequency range from 1 kHz to 10 MHz, and the voltage range from 0 to 0.24 V. The experimental results show that the ϵ' , ϵ'' and $\tan\delta$ values decrease with increasing frequency while σ_{ac} , M' and M'' values increase. This results will show that dielectric parameters are strongly frequency dependent.

Keywords V₂O₅ thin film · Dielectric properties · Interface state density · Anodic surface passivation

1 Introduction

V₂O₅ is a transition metal oxide semiconductor that has attracted considerable interest for its potential in catalysis [1], actuators [2], gas sensors [3], optical electronic devices [4], electrochemical supercapacitors [5] and an attractive material for rechargeable lithium-ion batteries due to its high electrochemical activity, stability and energy density [6]. V₂O₅ is a polycrystalline material and has a layered

orthorhombic structure [7]. Many techniques have been used to prepare V₂O₅ thin films. Some of these techniques are sputtering [8], sole gel technique [9], chemical vapor deposition [10], electrochemical deposition [11] and hydrothermal synthesis [12]. Among these techniques, spray pyrolysis is a preferred chemical method for producing large-area homogeneous thin films due to its simplicity and low cost. [13, 14]. Vanadium oxide films of different stoichiometry, with a wide range of stable oxidation states, can be easily fabricated by varying the sputtering parameters. These parameters are scanning speed, substrate temperature, distance between substrate and nozzle, carrier gas, and solution flow rate. It is possible that vanadium oxide thin films could be used as an interface layer in metal semiconductor diodes. The electrical properties of the junction are significantly affected by this layer, as well as the density of interface states at the junction. In addition, the dielectric parameters of the diode are dominated by the thickness of the interfacial layer. Creating an interfacial layer such as V₂O₅ in the junction can increase its diode's stability and performance. This is because this layer reduces the

✉ Elvan Şenarslan
elvan@atauni.edu.tr

¹ Aşkale Vocational School of Higher Education, Department of Electricity and Energy, Atatürk University, Erzurum, Turkey

² Graduate School of Natural and Applied Sciences, Department of Nanoscience and Nanoengineering, Atatürk University, Erzurum, Turkey

³ Faculty of Science, Department of Physics, Atatürk University, Erzurum, Turkey

dislocations present and the size of the defects on the semiconductor surface [15, 16].

Furthermore, research has been published on various aspects of perovskite solar cells, including challenges and strategies related to device functional layers and their integration into high-performance inorganic perovskite solar cells [17], functional layers of inverted flexible perovskite solar cells and effective technologies for device commercialization [18], mixed halide inorganic perovskite solar cells: opportunities and challenges [19], and strain engineering for high-performance formamidinium-based perovskite solar cells [20].

By including the interface between metal/semiconductor (MS) diodes, metal/insulator/semiconductor (MIS) diodes can be created. Moreover, the physical and electrical properties of MIS diodes are highly dependent on the surface preparation conditions and the formation of the interfacial layer [21]. The dielectric properties of MIS diodes are influenced by a variety of parameters. The factors to be considered are the preparation method of the materials, the height of the barrier between the metal and the semiconductor, the trap density at the interface, the series resistance of devices, the formation and thickness of the interfacial layer, and its homogeneity [22]. Ideally, the capacitance of MS and MIS diodes remains independent of frequency, especially at frequencies exceeding 1 MHz. But, depending on the frequency of the AC signal, there may be additional capacitance due to interface states over depletion layer capacitance. This interfacial capacitance is highly dependent on frequency and voltage and is also known as excess capacitance [21, 22]. Therefore, it is crucial to consider the impact of both the voltage and the frequency when examining the electrical and dielectric characteristics of diodes. As it can be seen from the frequency response, the dielectric constant, dielectric loss, and loss tangent parameters show significant dispersion at low frequencies [23]. In addition, numerous defects and impurities are created on the surface of the semiconductor due to the periodic interruption of the lattice structure on the surface. Consequently, energy levels are formed that correlate with the interface states found within the bandgap of the semiconductor. These energy levels are affected significantly by the temperature, voltage, and frequency applied to the device. Therefore, there should be interfacial layers with perfect homogeneity [24–26]. Also, surface passivation at the metal-semiconductor rectifier junction is extremely important. This is because the properties of the surface have a significant impact on the performance of this junction. Since the electrical properties of semiconductor devices are highly sensitive to impurities, they can change unpredictably over time. Therefore, passivation of the semiconductor surface is one way of eliminating this undesirable surface condition. As a consequence of

reducing the electrical activity on the surface of the semiconductor through the process of passivation, the device's stability and performance may be enhanced [26, 27]. Our previous study [28] provides a detailed investigation of the optical, morphological, and nanostructural properties of a vanadium oxide thin film grown with spray pyrolysis.

This article is concerned with the frequency-dependent investigation of the electrical and dielectric properties of Al/p-type Si/Al and Al/V₂O₅/p-type Si/Al diodes with and without passivation of the semiconductor surface by anodic oxidation. Our research presents a practical, low-cost, and uncomplicated method. This is an easy, inexpensive, and simple method.

2 Experimental details

The diodes fabricated for this study were made from a 400 μm thick p-type silicon wafer with surface orientation (100), carrier density $2.5 \times 10^{17} \text{ cm}^{-3}$, and resistivity 1–10 Ω cm. Initially, the p-Si semiconductor was chemically cleaned according to standard cleaning methods [28, 29]. Then it was placed in a vacuum deposition unit with its back surface facing up, and aluminum metal was evaporated onto the surface at a pressure of about 10^{-6} Torr. Later, the semiconductor was annealed in the N₂ atmosphere at 580 °C for 3 min. Afterward, it was divided into 4 equal parts to investigate the influence of surface passivation on the C-f properties of diodes with and without a V₂O₅ interface layer. The four samples were named as follows:

1. D1: Al/p-type Si/Al reference diode which is not passivated.
2. D2: Al/p-type Si/Al reference diode which is passivated.
3. D3: Al/V₂O₅/p-type Si/Al diode with V₂O₅ interface layer which is not passivated.
4. D4: Al/V₂O₅/p-type Si/Al diode with V₂O₅ interface layer passivated.

To obtain the D1, the first part was immediately put into a vacuum coating unit. Aluminum spots with a contact area of $7.85 \times 10^{-3} \text{ cm}^2$ were produced on the polished surface of the p-Si semiconductor by evaporation at about 10^{-6} Torr. As a result, the D1 diode was obtained.

The second part of the semiconductor was anodically passivated to obtain the D2 diode. For this, 0.1 M potassium hydroxide (KOH) as the electrolyte, an Al/p-Si wafer as the anode, and a platinum plate as the cathode were used.

The pH of the solution was measured and found to be 5. By applying a constant current density of 10 mA/cm², a SiO₂ film was formed. Following this, a dilute hydrofluoric acid (15:1 H₂O-HF) solution was used to remove the

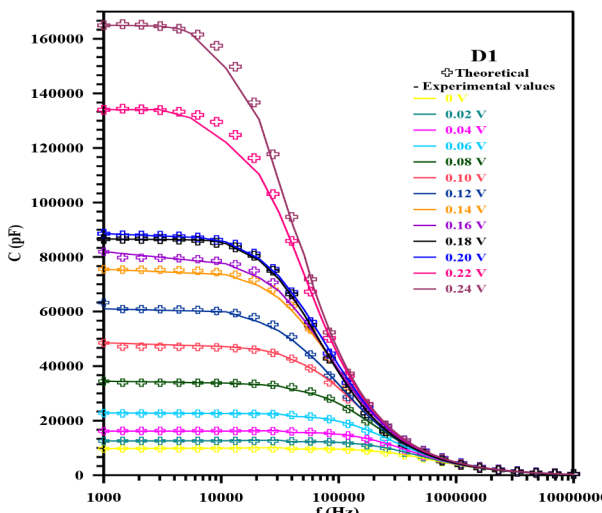


Fig. 1 Forward and reverse bias C - f characteristics of D1 diode at different voltages

SiO_2 layer from the semiconductor's surface. By repeating this procedure ten times, the number of imperfections and unsaturated bonds on the semiconductor's surface was decreased. Afterward, aluminum dots with a contact area of $7.85 \times 10^{-3} \text{ cm}^2$ were produced by evaporating aluminum metal at about 10^{-6} Torr on the passivated surface of the p-type silicon semiconductor. As a result, a passivated diode D2 is obtained.

To obtain the D3 diode, a V_2O_5 thin film was grown by spraying 0.1 M VCl_3 solution on the third semiconductor part with aluminum ohmic contacts using the spray pyrolysis method. For this purpose, the solution was sprayed onto the semiconductor substrate at an angle of 90° in the spray pyrolysis thin film production system, with doping times ranging from 5 to 10 min on the semiconductor substrate, after the flow rate was set to 5 ml/min, the flow factor to 2, the substrate nozzle distance to 22 cm and the substrate temperature to 450°C . Then, aluminum dots with a contact area of $7.85 \times 10^{-3} \text{ cm}^2$ on this thin film were evaporated in a vacuum coating unit. Thus, a D3 diode with interface layer and non-passivated surface was obtained.

To obtain the D4 diode, the fourth part of the semiconductor was anodically passivated using the method described for the D2 diode. Subsequently, a V_2O_5 thin film was formed on the passivated surface using the method detailed in the fabrication of the D3 diode. Finally, to obtain aluminum dots with a contact area of $7.85 \times 10^{-3} \text{ cm}^2$, the special Al/p-Si/ V_2O_5 structure was placed in a vacuum unit, and aluminium metal was evaporated at a pressure of 10^{-6} Torr. Thus, a D4 diode with both V_2O_5 interfacial layer and anodic passivation was obtained.

C - f measurements of these diodes in the frequency range 1 kHz to 10 MHz were taken in the dark and at room

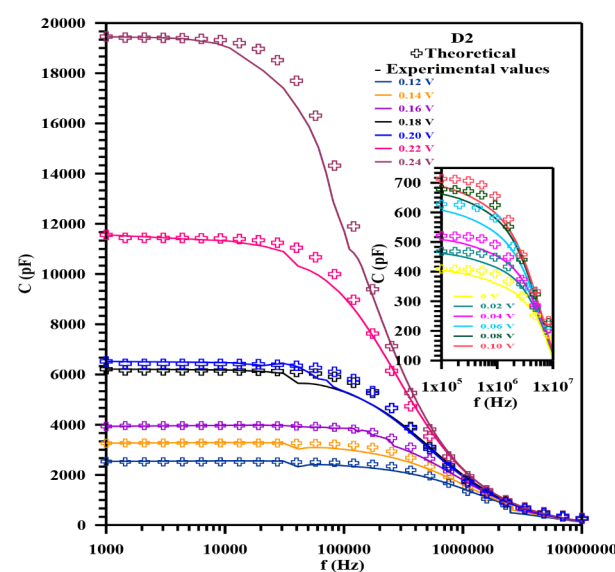


Fig. 2 Forward and reverse bias C - f characteristics of D2 diode at different voltages

temperature using an HP 4142 A (50 Hz-13 MHz) LF impedance analyzer. Several dielectric parameters were calculated and compared.

3 Results and discussion

3.1 Determination of interface state density (N_{ss}) and time constant (τ) values from C - f characteristics of D1, D2, D3, and D4 diodes

The theoretical and experimental C - f characteristics of D1 and D2 diodes are given in Figs. 1 and 2 as a function of frequency at different bias voltages at room temperature. Similarly, for diodes D3 and D4, these characteristics are given in Figs. 3 and 4, respectively. From the C - f characteristics ranging from 1 kHz to 10 MHz, it can be seen that the measured capacitance decreases with increasing frequency and remains almost constant up to a certain value of the frequency at low frequencies. The capacitance is higher at low frequencies due to excess capacitance resulting from the interfacial states in equilibrium with the p-Si, which can follow the AC signal. At first, the capacitance values of the diodes decrease steeply with increasing frequency and then become frequency-independent, especially above 1 MHz. This is because at high frequencies only a small proportion of the interface states can follow the signal, so their contribution to the capacitance was very small, and in this case the diodes only have a capacity for space charge. The presence of the V_2O_5 interface layer resulted in higher capacitance values in D3 and D4 samples, especially at low-frequencies.

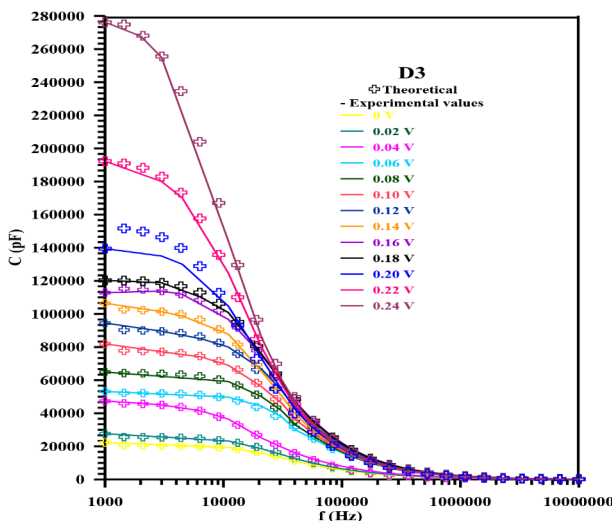


Fig. 3 Forward and reverse bias C - f characteristics of D3 diode at different voltages

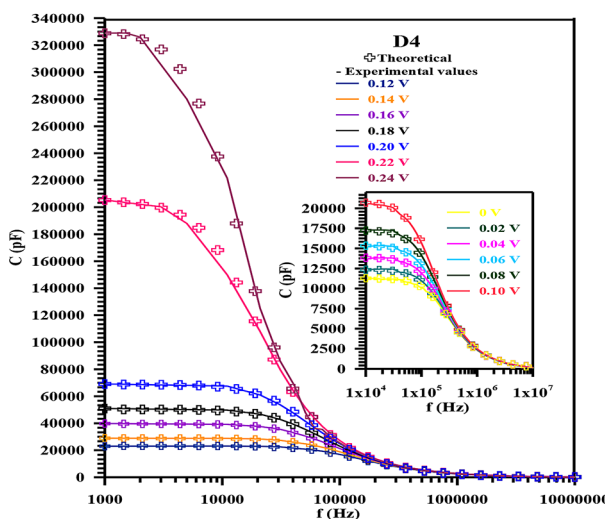


Fig. 4 Forward and reverse bias C - f characteristics of D4 diode at different voltages

At the same time, surface passivation caused a rapid decrease in capacitance (in the low frequency region) with decreasing bias voltage. This is seen in the graphs given in the inset of Figs. 2 and 4.

The density of interfacial states is another parameter that plays an important role in the characteristics of the diode. The energy of the interfacial state compared to the valence band top for a p-type semiconductor is given by [30]

$$E_{ss} - E_v = q\phi_b - qV \quad (1)$$

where E_v is the valence band edge and E_{ss} is the energy of interface states N_{ss} expressed as the density of the interfacial state in equilibrium with the semiconductor.

Capacity depending on frequency is given by [31].

$$C = C_{it} + C_{sc} \text{ (at low frequencies)} \quad (2)$$

$$C = C_{it} \text{ (at high frequencies)} \quad (3)$$

where C is the total capacitance and C_{sc} is the capacitance of the depletion region.

The capacitance accompanying the interface states is given by [32]

$$C_{it} = SqN_{ss} \frac{\arctan(\omega\tau)}{\omega\tau} \quad (4)$$

where ω is the angular frequency, τ is the relaxation time constant and S is the effective area of the diode. **Also, time constant of interface states** is given by [33]

$$\tau = \frac{1}{v_{th}\sigma N_a} \exp\left(\frac{qV_d}{kT}\right) \quad (5)$$

Where σ is the cross-section of interface states, v_{th} is the thermal velocity of the carrier and N_a is the doping concentration.

The interfacial state density and time constant values were obtained by fitting the experimental values of the forward bias C - f to the theoretical C - f values using Eqs. (2) and (3). Tables 1 and 2 give experimental values of some basic parameters derived from the C - f characteristics of the Al/p-Si/Al and Al/V₂O₅/p-Si/Al diodes with and without anodic passivation, respectively. Using these values, the changes in N_{ss} and τ versus the interfacial state energy given by Eq. (1) are shown in Figs. 5, 6, 7 and 8. As can be seen from Figs. 5, 6, 7 and 8, the interfacial state density and relaxation time constant show a decrease as the interfacial state energy increases. While N_{ss} values in D1, D3, and D4 samples are in the range of 10^{13} - 10^{14} eV⁻¹cm⁻², it is in the range of 10^{12} - 10^{13} eV⁻¹cm⁻² in the D2 sample. These values of the interface states are high enough to pin the Fermi level of the Si substrate surface [31, 34]. Again, τ values were found in the order of about 10^{-5} - 10^{-6} s for four samples and were seen to be consistent with the values given in the literature.

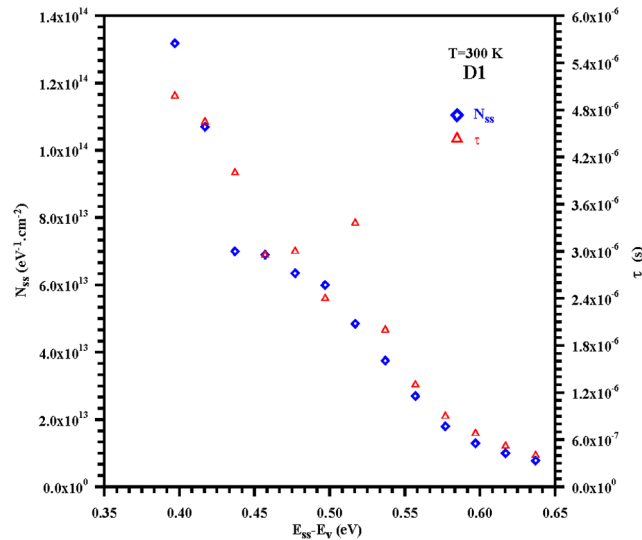
For both types of anodically passivated samples, the interfacial density of states has shifted slightly towards the mid-gap and decreased.

3.2 Determination of dielectric parameter values of D1, D2, D3, and D4 diodes depending on application frequency and bias

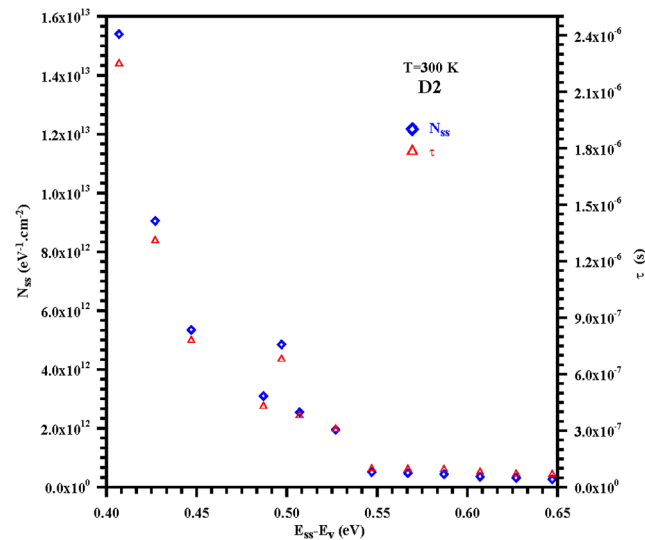
It is known from basic physics courses that electrical conductivity is related to the movement of free electrons, while

Table 1 Experimental values of some basic parameters derived from the $C-f$ characteristics of the D1 and D2 diodes

	$E_{ss}-E_v$ (eV)	N_{ss} ($eV^{-1}cm^{-2}$)	τ (s)
D1	0.397	1.32×10^{14}	4.98×10^{-6}
	0.417	1.07×10^{14}	4.65×10^{-6}
	0.437	7.00×10^{13}	4.00×10^{-6}
	0.457	6.90×10^{13}	2.95×10^{-6}
	0.477	6.35×10^{13}	3.00×10^{-6}
	0.497	6.00×10^{13}	2.40×10^{-6}
	0.517	4.85×10^{13}	3.36×10^{-6}
	0.537	3.75×10^{13}	2.00×10^{-6}
	0.557	2.70×10^{13}	1.30×10^{-6}
	0.577	1.80×10^{13}	9.00×10^{-7}
	0.597	1.29×10^{13}	6.80×10^{-7}
	0.617	1.00×10^{13}	5.20×10^{-7}
	0.637	7.80×10^{12}	4.00×10^{-7}
D2	0.407	1.54×10^{13}	2.25×10^{-6}
	0.427	9.05×10^{12}	1.31×10^{-6}
	0.447	5.35×10^{12}	7.80×10^{-7}
	0.497	4.85×10^{12}	6.80×10^{-7}
	0.487	3.10×10^{12}	4.30×10^{-7}
	0.507	2.55×10^{12}	3.80×10^{-7}
	0.527	1.95×10^{12}	3.08×10^{-7}
	0.547	5.15×10^{11}	9.80×10^{-8}
	0.567	4.84×10^{11}	9.60×10^{-8}
	0.587	4.42×10^{11}	9.40×10^{-8}
	0.607	3.60×10^{11}	8.00×10^{-8}
	0.627	3.18×10^{11}	7.00×10^{-8}
	0.647	2.70×10^{11}	6.80×10^{-8}

**Fig. 5** The energy-distribution curves of the interfacial state density and time constants obtained from $C-f$ characteristics for the D1 diode at room temperature**Table 2** Experimental values of some basic parameters derived from the $C-f$ characteristics of the D3 and D4 diodes

	$E_{ss}-E_v$ (eV)	N_{ss} ($eV^{-1}cm^{-2}$)	τ (s)
D3	0.564	2.24×10^{14}	2.56×10^{-5}
	0.584	1.54×10^{14}	1.96×10^{-5}
	0.604	1.22×10^{13}	1.84×10^{-5}
	0.624	9.60×10^{12}	9.50×10^{-6}
	0.644	9.20×10^{12}	9.50×10^{-6}
	0.664	8.20×10^{12}	1.01×10^{-5}
	0.684	7.20×10^{12}	8.30×10^{-6}
	0.704	6.20×10^{12}	8.20×10^{-6}
	0.724	5.12×10^{12}	7.10×10^{-6}
	0.744	4.16×10^{12}	6.10×10^{-6}
	0.764	3.68×10^{12}	1.51×10^{-5}
	0.784	2.04×10^{12}	8.80×10^{-6}
	0.804	1.65×10^{12}	7.10×10^{-6}
D4	0.581	2.64×10^{14}	1.00×10^{-5}
	0.601	1.63×10^{14}	1.02×10^{-5}
	0.621	4.00×10^{13}	2.86×10^{-6}
	0.641	3.15×10^{13}	2.65×10^{-6}
	0.661	2.29×10^{13}	2.35×10^{-6}
	0.681	1.85×10^{13}	1.70×10^{-6}
	0.701	1.65×10^{13}	1.30×10^{-6}
	0.721	1.37×10^{13}	1.30×10^{-6}
	0.741	1.22×10^{13}	1.00×10^{-6}
	0.761	4.16×10^{12}	9.80×10^{-7}
	0.781	1.10×10^{12}	9.00×10^{-7}
	0.801	9.80×10^{11}	8.00×10^{-7}
	0.821	8.95×10^{11}	7.00×10^{-7}

**Fig. 6** The energy-distribution curves of the interface states and time constants obtained from $C-f$ characteristics for the D2 diode at room temperature

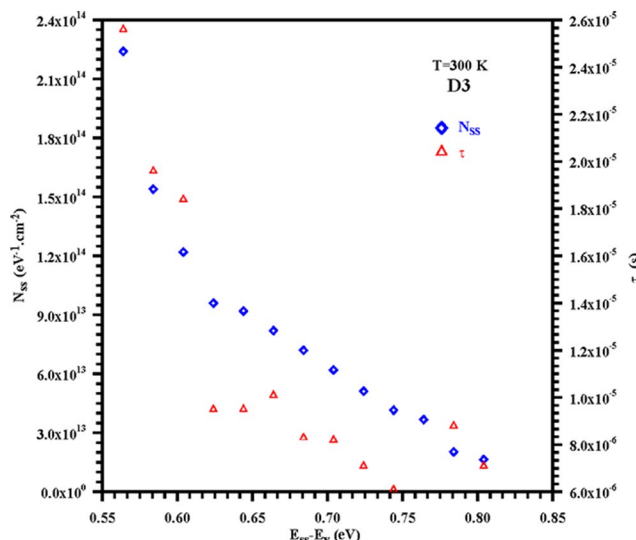


Fig. 7 The energy-distribution curves of the interface states and time constants obtained from $C-f$ characteristics for the D3 diode at room temperature

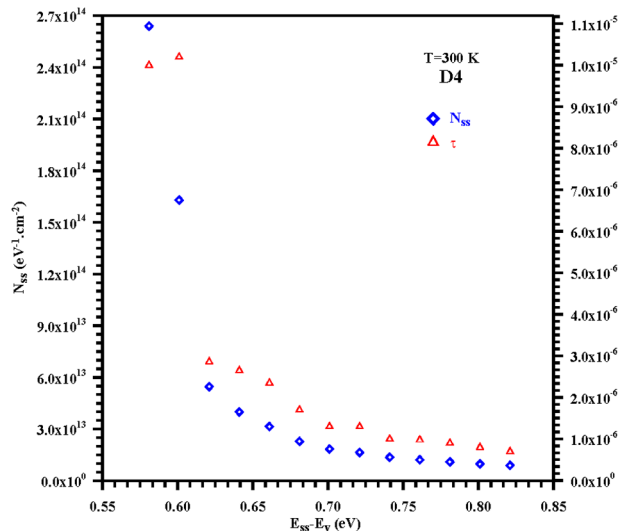


Fig. 8 The energy-distribution curves of the interface states and time constants obtained from $C-f$ characteristics for the D4 diode at room temperature

dielectric constants are related to the behavior of bound electrons. It can be said that the dielectric constant is a measure of the extent to which a substance concentrates lines of electrostatic flux. At the same time, the dielectric constant can be defined as the ratio of the amount of electrical energy stored in the insulator to the vacuum when a static electric field is applied to the dielectric material. Apart from the vacuum, the response of dielectric materials to external fields generally depends on the frequency of the imposed field. This frequency dependence arises because the polarization of a material does not respond immediately to an applied field. For this reason, the dielectric constant is expressed as

a complex function of the frequency of the applied field. The response of materials to alternating fields is characterized by a complex dielectric constant consisting of real and imaginary parts. Therefore, when an electric field is applied to a dielectric medium, it can be said that the current flowing through the actual dielectric is the sum of the conduction and displacement currents. Since there is very little free charge in good dielectrics, the conduction current is extremely small and the displacement current can be interpreted as the elastic response of the dielectric material to any change in the applied electric field. A displacement current flows with increasing electric field strength, and the additional displacement is stored as potential energy in the dielectric. But if the electric field decreases, then the dielectric releases some of the stored energy as displacement current. It can be said that there are two types of losses in all dielectrics, one of which is conduction loss and the other is dielectric loss. Conduction loss represents the actual flow of charge across the dielectric. Dielectric loss, on the other hand, results from the rotation or movement of atoms or molecules in an alternating electric field [35]. By examining various dielectric parameters, polarization and conduction mechanisms in dielectrics can be revealed.

Dielectric properties are associated with the properties of admittance spectroscopy. Admittance measurements can be obtained from a capacitance (C) parallel to a conductance (G). Many dielectric parameters can be calculated by taking into account the admittance data analysis method in the interface characterization of metal-semiconductor and metal-interface layer-semiconductor structures. Investigating the role of interfacial states in different polarization mechanisms in dielectric materials by considering $C-f$ characteristics in a wide frequency range can contribute to a better understanding of possible current conduction mechanisms through dielectric material. Similarly, investigating dielectric loss may also contribute to understanding the dissipation of energy in the form of heat within dielectric materials. The dielectric properties of Al/p-Si/Al and Al/ V_2O_5 /p-Si/Al structures produced with and without anodic passivation were examined by admittance spectroscopy technique at room temperature, in the frequency range of 1 kHz–10 MHz and under different positive bias voltages (0–0.24 V). (Fig. 1–10)

Depending on the capacitance and conductance values, the complex dielectric constant (ϵ^*) can be expressed as follows [24, 26, 35–37]:

$$\epsilon^*(\omega) = \epsilon' - i\epsilon'' = \frac{C}{C_0} - i\frac{G}{\omega C_0} \quad (6)$$

where ϵ' and ϵ'' are the real and imaginary components of complex dielectric constant, respectively. While the ϵ'

Fig. 9 Frequency dependence of ϵ' for (a) D1 (b) D2 diodes at different voltages

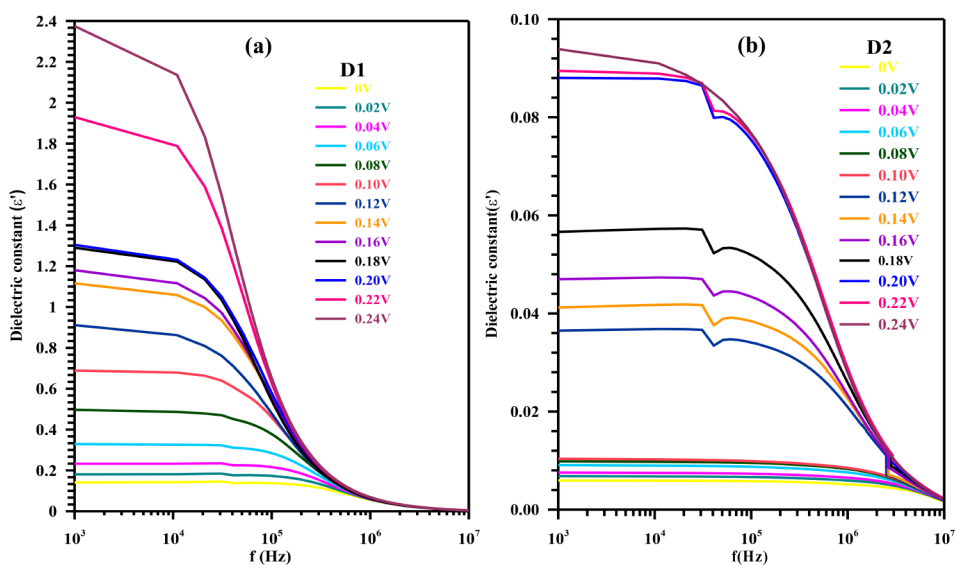
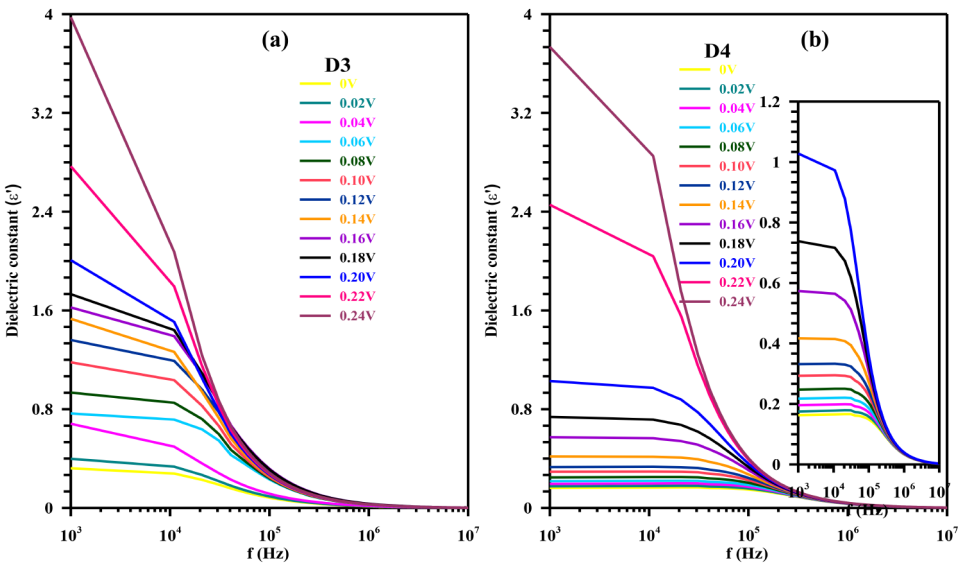


Fig. 10 Frequency dependence of ϵ' for (a) D3 (b) D4 diodes at different voltages



represents stored energy as well as dipole strength against the applied electric field and is called dielectric constant, the ϵ'' is dielectric loss and shows absorbed energy due to frictional dampening. Where i is the imaginary root of -1, ω is the angular frequency. Also, the measured capacitance and conductance values are C and G , respectively. C_0 is the capacitance of the capacitor without any dielectric and is given by $C_0 = \frac{\epsilon_0 S}{d}$, ϵ_0 is the permittivity of free space ($8.85 \times 10^{-12} \text{ F/m}$) and d is the thickness of the interlayer. Figure 9 (for D1 and D2) and 10 (for D3 and D4) demonstrate the frequency dependency of the dielectric constant for various voltages. It is apparent from these figures that the values of ϵ' show a significant decrease with increasing frequency for each voltage. The dielectric constant such as the interface properties has a significant effect on

the electrical parameters of diodes with and without surface passivation. In turn, these diodes exhibit diverse responses in the high and low- frequency regions. Although a nearly constant change was observed in the low- frequency range, these changes started to decrease in the mid- frequency range. Moreover, at high frequencies, it is almost frequency-independent. Generally, ϵ' values at low frequencies are influenced by four types of polarization processes: dipolar, ionic, electronic, and surface or interfacial polarization. Nevertheless, at high frequencies, polarisation processes other than electronic polarisation are ineffective. This means that only electronic polarisation contributes to the ϵ' values [38]. The reduction in ϵ' values as frequency increases suggests that the alignment of interface dipoles with the field direction requires less time, due to the very rapid change in

Fig. 11 Frequency dependence of ϵ'' for (a) D1 (b) D2 diodes at different voltages

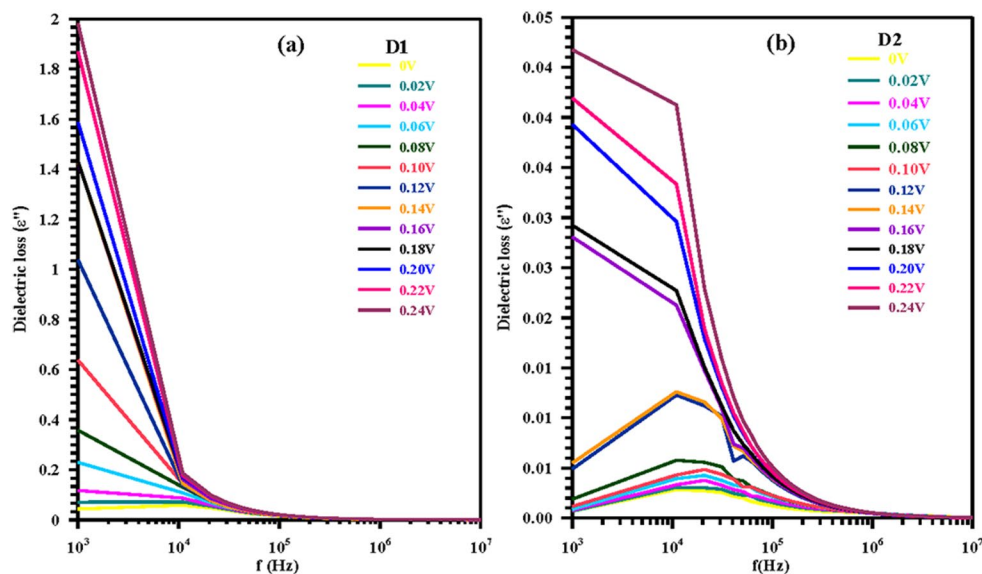
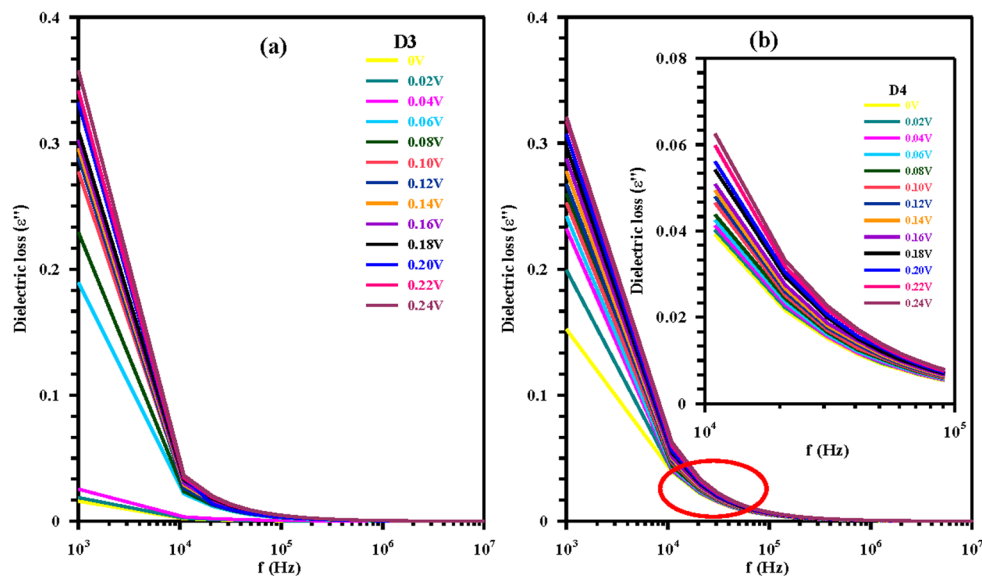


Fig. 12 Frequency dependence of ϵ'' for (a) D3 (b) D4 diodes at different voltages



the external alternating electric field [21, 39]. This causes the dielectric constant to decrease [40]. As a result of the polarization of the dielectric material under the influence of an external field at low and intermediate frequencies, the displacement of charges from traps or equilibrium states occurs. Therefore, it is clear that the relaxation time has an important role in changing the dielectric properties with the frequency of the applied external field.

The magnitude of ϵ'' is generally lower than that of ϵ' , and it is always greater than zero. It is desirable for any type of dipole that the dielectric loss is low at frequencies close to the relaxation frequency of the dielectric material under the electric field effect [40]. The frequency-dependent variation of the dielectric loss for different voltages is shown in Figs. 11–12. As can be seen from these figures, the frequency-dependent variation of ϵ'' shows the same behavior

as ϵ' . As stated above, the variation of ϵ'' with frequency is above zero but below ϵ' .

It is seen from the changes in ϵ' and ϵ'' that the real and imaginary components of the dielectric constant decrease as the frequency and voltage increase. ϵ'' and ϵ'' exhibit almost no voltage dependence in the inversion region. However, in the depletion and accumulation regions, there is a strong dependence observed on frequency and voltage. This variation may be due to charge effects from charged carriers trapped in interface states.

The loss tangent, which is sometimes called the dissipation factor and is symbolised as $\tan\delta$, is the ratio of the dielectric loss to the dielectric constant [24, 35–39]:

$$\tan\delta = \frac{\epsilon''}{\epsilon'} \quad (7)$$

Fig. 13 Frequency dependence of $\tan\delta$ for (a) D1 (b) D2 diodes at different voltages

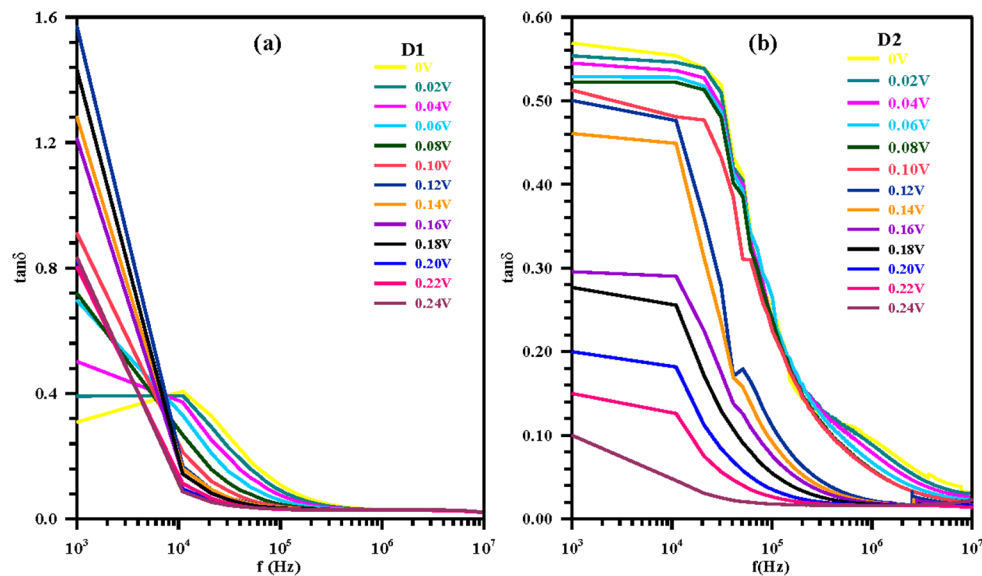


Fig. 14 Frequency dependence of $\tan\delta$ for (a) D3 (b) D4 diodes at different voltages

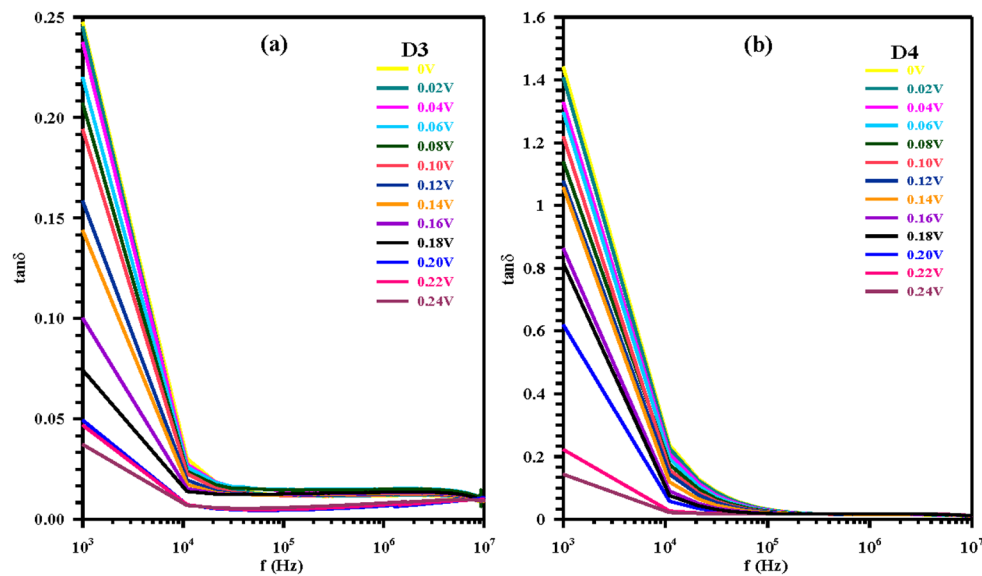


Figure 13 (for D1 and D2) and 14 (for D3 and D4) show $\tan\delta$ versus frequency plots for diodes with and without an interfacial layer. As can be seen from these figures, the $\tan\delta$ decreases with increasing frequency in the frequency range from 1 kHz to 1 MHz and then becomes frequency - independent, especially at frequencies above 1 MHz. That is, the $\tan\delta$ values are also almost voltage-independent in the inversion region, while at low frequencies they are strongly frequency and voltage-dependent in the depletion and accumulation regions. This dependence can be attributed to the differing response times of interface states and reversal loads at high and low frequencies. (Fig. 14)

The frequency dependence of the loss tangent can also be discussed according to the frequency-dependent changes of ϵ' and ϵ'' values [41]. Thus, the frequency dependence of the loss tangent can be interpreted by the Maxwell-Wanger

interfacial polarization (i.e., hopping frequency is similar to external electric field frequency) [42]. Interfacial polarization is produced by the separation of moving positively and negatively charged particles under an applied field, creating positive and negative space charges at the interfaces between different materials. These space charges, in turn, modify the field distribution. The process of transport of charge carriers in interfacial polarization occurs in three ways: hopping, fast ionic conduction, and diffusion. Interfacial polarization occurs as a result of the separation of positive and negative charges in the dielectric medium. Interfacial polarization is also called Maxwell-Wagner polarization. Hopping polarization occurs when electrons and holes, ions, and vacancies hop from one region to another. Polarization will occur on the application of a reversing electric field, but will not follow the reversals exactly, since polarization takes a finite

Fig. 15 Frequency dependence of σ_{ac} for (a) D1 (b) D2 diodes at different voltages

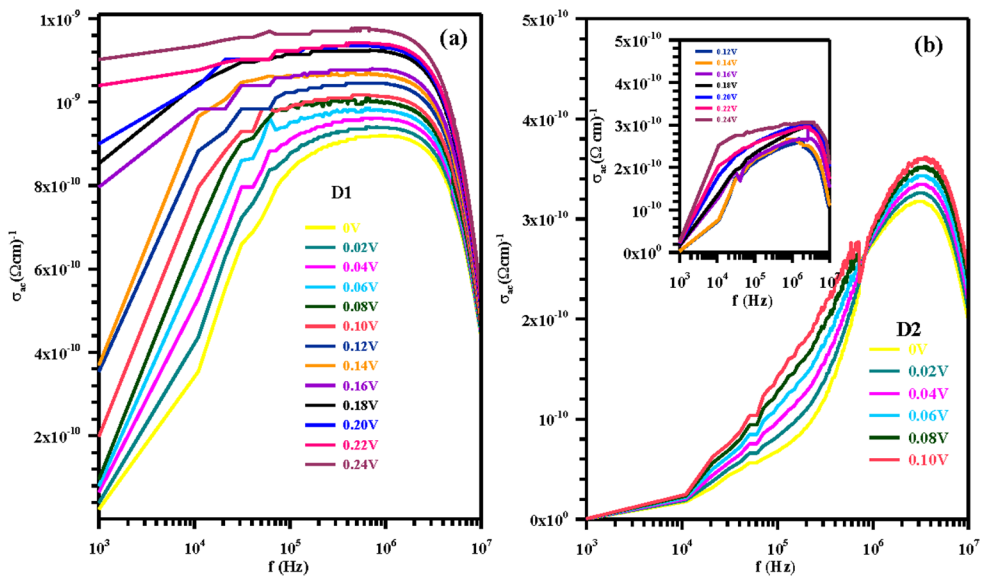
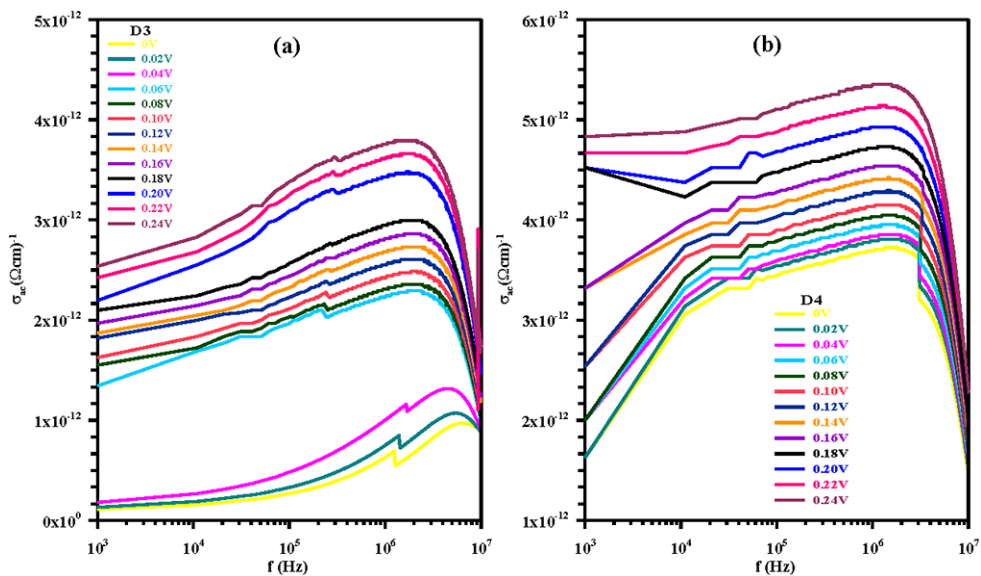


Fig. 16 Frequency dependence of σ_{ac} for (a) D3 (b) D4 diodes at different voltages



time. In general, interfacial polarization mechanisms are the slowest compared to molecular, ionic, and electronic polarization mechanisms. In other words, they have the response time with the longest time constant. It is the variation of this time constant that governs the effect of frequency on dielectric properties. As the frequency increases (shorter field reversal), the factors that cause slower polarization decrease, and therefore both the dielectric constant and the loss tangent decrease [43, 44]. Therefore, the variations of ϵ' , ϵ'' , and $\tan\delta$ with frequency can be interpreted as the fact that the high-frequency dipoles do not have enough time to orient themselves in the direction of the external AC signal. $\tan\delta$ values, which are large in the low or medium frequency range, start to decrease as the frequency increases in the high-frequency range. After a certain frequency value of the applied electric field, the interfacial polarization reached

a constant value, and in this case, most of the dipoles could not follow the AC signal [45].

The AC electric conductivity (σ_{ac}) is obtained from the dielectric loss values and can be calculated with the following equation, which depends on the ϵ'' values [24, 35–39].

$$\sigma_{ac} = \omega C \tan\delta \left(\frac{d}{A} \right) = \epsilon'' \omega \epsilon_0 \quad (8)$$

The experimental σ_{ac} - f graphs under a change in forward-bias voltage are shown in Figs. 15 and 16. These figures demonstrate the rise in σ_{ac} as frequency increases for nearly all applied biases at low and intermediate frequencies. The rise in electrical conductivity can be attributed to the increase in eddy currents. At high frequencies, the

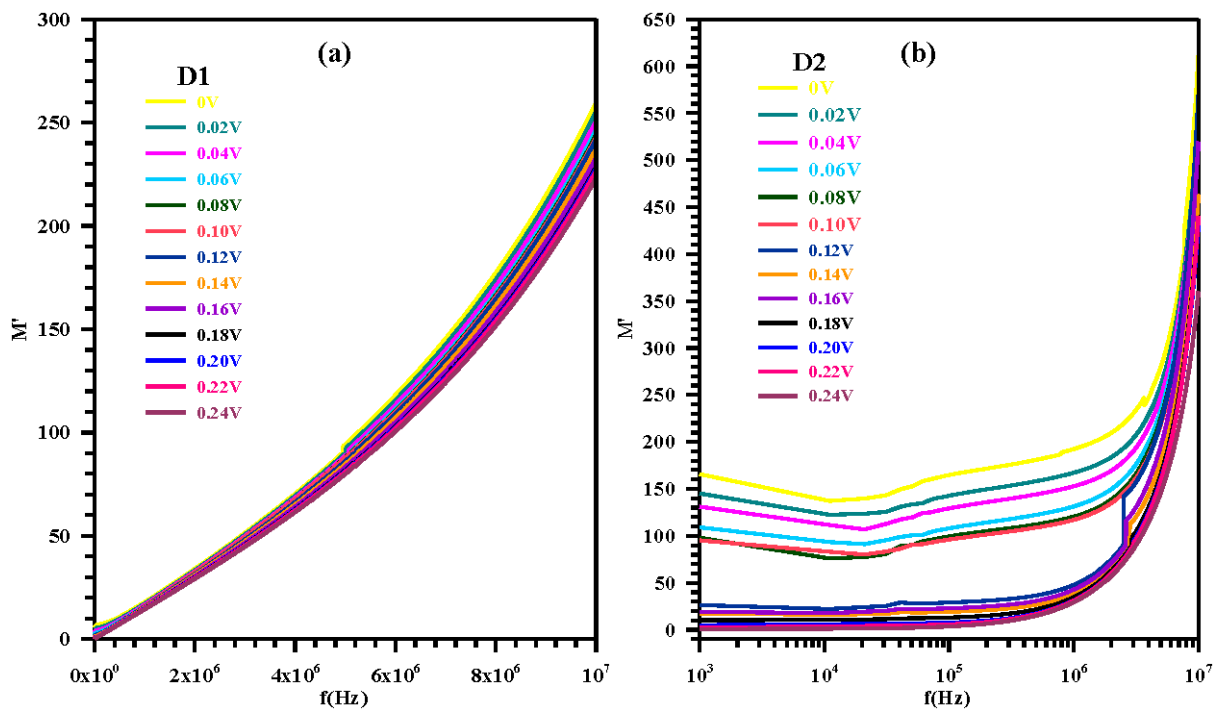


Fig. 17 Frequency dependence of M' for (a) D1 (b) D2 diodes at different voltages

conductivity values relate to ac conductivity, while at low frequencies, it involves dc conductivity (σ_{dc}) [46, 47].

The complex electric modulus (M^*) is another crucial parameter to understand the polarisation and relaxation process in ionic-electronic conducting materials. The physical interpretation of the electric modulus can be expressed as corresponding to the relaxation of the electric field in the material when the electric displacement vector remains constant. Therefore, it can be said that the modulus represents the actual dielectric relaxation process. Accordingly,

at low frequencies, the change at large values of the dielectric constant and conductivity is minimized. Thus, general difficulties obscuring relaxation in dielectric constant representation can be resolved [46].

The real part (M') and imaginary part (M'') parameters both contribute to the complex electric modulus (M^*), which can be expressed as follows:

$$M^* = M' + iM'' \quad (9)$$

Fig. 18 Frequency dependence of M' for (a) D3 (b) D4 diodes at different voltages

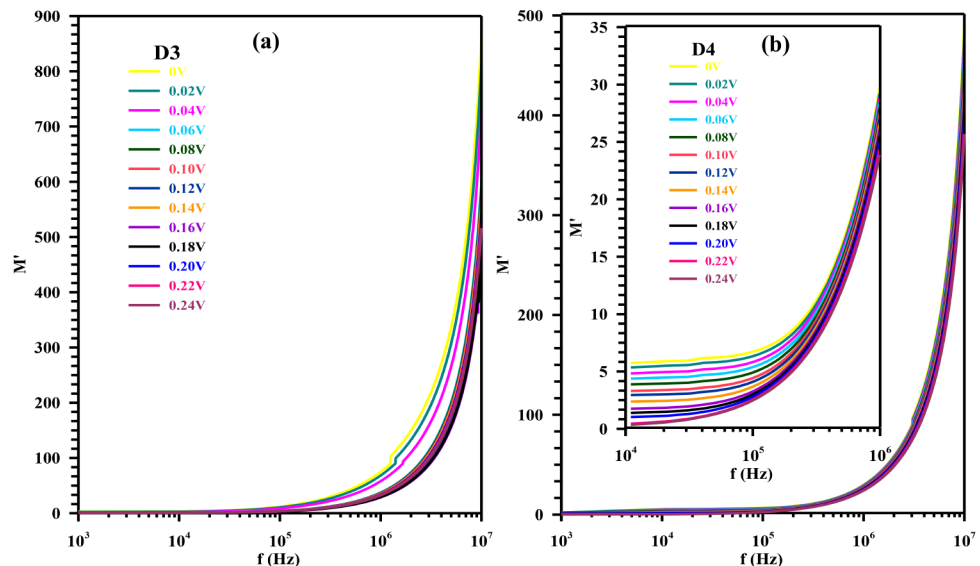
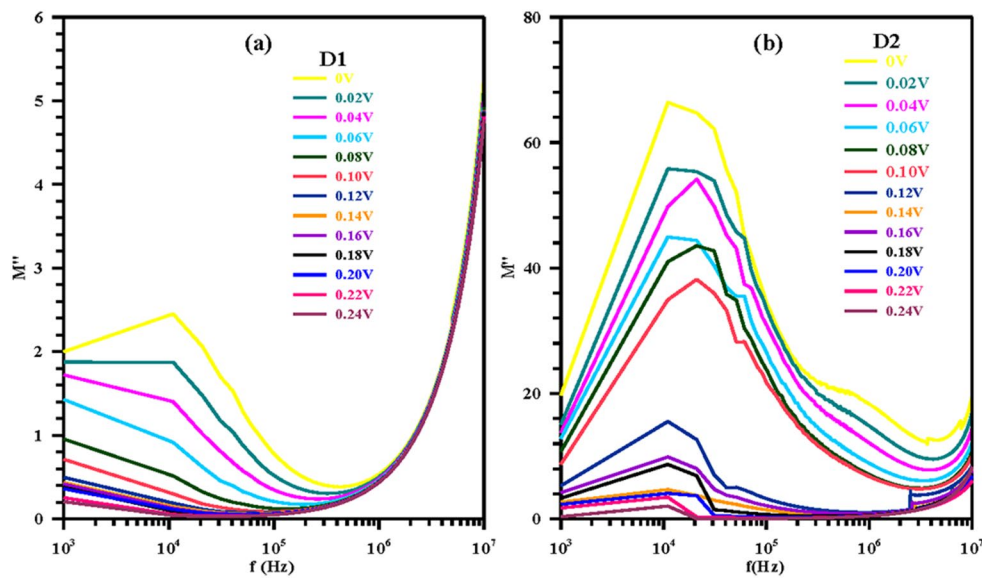


Fig. 19 Frequency dependence of M'' for (a) D1 (b) D2 diodes at different voltages



The M' and M'' values can be written as the next formula related to the ϵ' and ϵ'' values: and are calculated from ϵ' and ϵ'' data as:

$$M^* = \frac{1}{\epsilon^*} = \frac{\epsilon'}{\epsilon'^2 + \epsilon''^2} + i \frac{\epsilon''}{\epsilon'^2 + \epsilon''^2} = M' + iM'' \quad (10)$$

The actual (M') and the imaginary (M'') components of M^* were obtained from ϵ' and ϵ'' by Eq. (10). Figures 17–20 shows the frequency dependence in the voltage range 0 V to 0.24 V of the real and imaginary components of the electric modulus for the fabricated diodes. It is seen from Figs. 17–18 that the real part M' of the complex electric modulus increases with increasing frequency and decreases almost exponentially with the increase of the applied bias voltage. These changes align with the M' values reaching a

maximum constant that corresponds to $M_\infty = 1/\epsilon_\infty$ due to relaxation. M' values reduce to zero at low frequencies and confirm the removal of electrode polarization [21]. It can be said that these changes become more evident in depletion and accumulation regions due to the existence of interface/dipole polarization and the fact that surface states depend on relaxation or lifetime at low/intermediate frequencies and series resistance at high frequencies. At the same time, M' approaches zero in the positive bias region at low frequencies, and this result indicates that electrode polarization leads to a negligible contribution to M^* and can be ignored when data are analyzed in this form [48, 49]. Therefore, it can be stated that interface/surface and dipole polarization are effective from low frequencies up to several hundred kHz, while ionic and electronic polarization are effective at very high frequencies. The increase in frequency causes

Fig. 20 Frequency dependence of M'' for (a) D3 (b) D4 diodes at different voltages

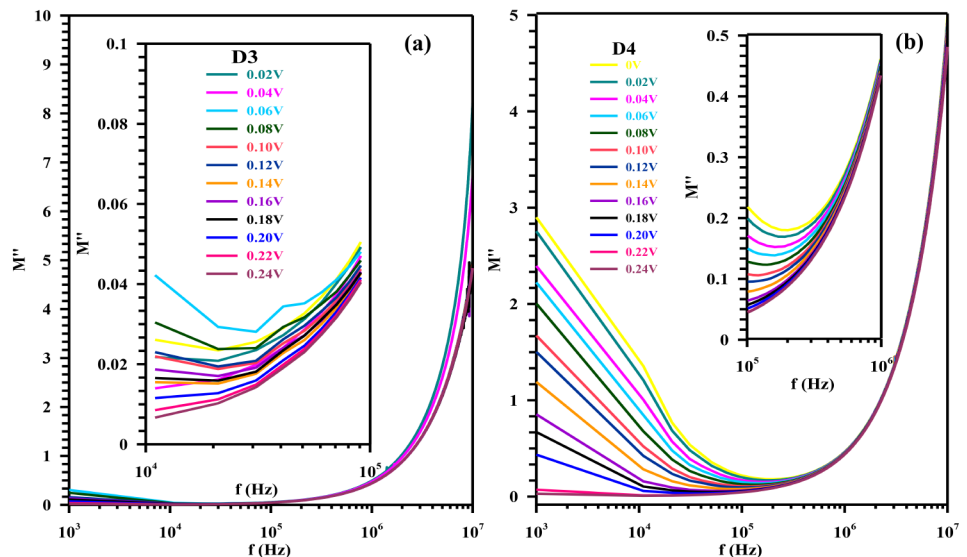


Table 3 A comparison of the values of dielectric parameters such as ϵ' , ϵ'' , $\tan\delta$, σ_{ac} , M' and M'' calculated for Al/p-Si/Al and Al/V₂O₅/p-Si/Al structures with some samples in the literature. The comparison was made using 10 kHz and 1 MHz application frequencies at 1 V positive bias voltage

Sample	ϵ'		ϵ''		$\tan\delta$		$\sigma_{ac} (\Omega \text{cm})^{-1}$		M'		M''		Refs.	
	1 V		1 V		1 V		1 V		1 V		1 V			
	10	1	10	1	10	1	10	1	10	1	10	1		
	kHz	MHz	kHz	MHz	kHz	MHz	kHz	MHz	kHz	MHz	kHz	MHz		
Al/p-Si/Al (D1)	0.7	0.065	0.144	0.0018	0.213	0.0288	9.66×10 ⁻¹⁰	1.06×10 ⁻⁹	1.41	15.389	0.30	0.44	This work	
Al/V ₂ O ₅ /p-Si/Al (D3)	1.04	0.028	0.024	0.00034	0.023	0.0122	1.8×10 ⁻¹²	2.4×10 ⁻¹²	0.965	35.96	0.219	0.44	This work	
Al/SiO ₂ /p-Si	3.93	1.92	0.21	0.06	0.052	0.049	0	4×10 ⁻⁸	-	-	-	-	[53]	
Al/rubrene/p-Si	2.6	2.5	0.9	0.02	0.35	0.02	2×10 ⁻⁶	0	0.35	0.42	0.125	0.02	[54]	
Al/SiO ₂ /p-Si	0.64	0	0.29	0	0.45	0.15	1.6×10 ⁻⁹	3×10 ⁻⁹	-	-	-	-	[55]	
Al/P3HT/n-Si	7.6	2.8	55	4	7	1.8	5×10 ⁻⁸	16×10 ⁻⁸	0	0.2	0.02	0.026	[51]	
Al/HfO ₂ /p-Si	2.5	0	18	4	7.5	2	8×10 ⁻⁸	12×10 ⁻⁸	0	3.5	0	3.5	[56]	
Al/(PVA/Ni, Zn acetates)/n-Si	3	1	20	0	10	0	2.5×10 ⁻⁸	4×10 ⁻⁸	0	2	0.2	0.6	[57]	
Au/(Ag:ZnO)-PVP/n-Si	1.6	0.8	2.36	1.8	2	1.4	5×10 ⁻⁸	40×10 ⁻⁸	0.2	1	0.25	1.3	[58]	
Au/PVC+TCNQ/p-Si	1.08	0.12	0.48	0	0.46	0.06	-	-	1.6	11.2	0.7	0.6	[59]	
Al/TiO ₂ /p-Si	30	6	600	100	20	7	-	-	-	-	-	-	[60]	

an increase in the energy of the charge carriers and therefore leads to increased relaxation times [50, 51]. The M'' -changes of D1 and D2 diodes are consistent with many studies in the literature [39, 48, 50, 52]. However, M'' - f changes of D3 and D4 diodes correspond with the study in the literature [21]. While M'' increases from 1 kHz to 10 kHz, it decreases from 10 kHz to 100 kHz. Figures 19 and 20 shows the variation of the frequency dependence of M'' for different voltages. It can be observed from these figures that, as frequency increases, M'' increases and reaches a peak value at every bias voltage at 10 kHz. With increasing gate voltage, the peak shifts to a higher frequency. Additionally, there is an increase in M'' between 100 kHz and 10 MHz.

A comparison of the values of dielectric parameters such as ϵ' , ϵ'' , $\tan\delta$, σ_{ac} , M' and M'' calculated for Al/p-Si/Al and Al/V₂O₅/p-Si/Al structures with some samples in the literature is presented in Table 3. The comparison was made using 10 kHz and 1 MHz application frequencies at 1 V positive bias voltage. Since the samples presented in Table 3 consist of different materials, it can be seen that the dielectric parameter values calculated for these samples are different from each other. However, it can still be said that the parametric values calculated for the samples used in this study are compatible with the values calculated in the literature in terms of orders of magnitude.

4 Conclusion

While fabricating the diodes, the semiconductor surfaces were passivated by the anodic oxidation method. To fabricate the interface layered diodes, V₂O₅ thin films were deposited on the clean and polished surfaces of the p-Si semiconductor by chemical spraying technique. First, the effects of anodic surface passivation on the $C-f$ characteristics of Al/p-Si/Al and Al/V₂O₅/p-Si/Al diodes were evaluated. For each diode produced, the changes in the interfacial state density and time constant according to the interfacial state energy were determined. It is seen that the interfacial state density and time constant decrease as the interfacial state energy increases. This was attributed to the decrease in the number of unsaturated bonds and defect density in the Si semiconductor due to the effect of anodic passivation. Furthermore, the complex dielectric constant's real components (ϵ') and imaginary components (ϵ''), loss tangent ($\tan\delta$), AC conductivity (σ_{ac}), the complex electric modulus's real components (M') and imaginary components (M'') of these diodes have been examined by $C-f$ characteristics between 1 kHz and 10 MHz frequency at room temperature. It was shown that dielectric properties of the Al/p-Si/Al and Al/V₂O₅/p-Si/Al diodes with and without anodic passivation were found to be strongly dependent on frequency, especially at low

frequencies. This means that the capacitance values of the diodes produced are higher at low frequencies than at high frequencies. This behavior is attributed to the surface states can easily follow the AC signal, at low frequencies and yield an excess capacitance, which depends on the relaxation time of the surface states and the frequency of AC signal. When interfacial states exist at the metal-semiconductor junction interface, the device behaves differently than the ideal case. Since the interface capacitance (excess capacitance) resulting from these states is strongly dependent on frequency and applied voltage, the dielectric parameters determined from the $C-f$ characteristics are also strongly affected by the frequency of the applied AC signal. Dipolar groups in the dielectric can follow the low-frequency electric field, but it becomes difficult for these dipoles to follow the relatively fast, time-varying high-frequency electric fields, and therefore the values of parameters such as ϵ' , ϵ'' , $\tan\delta$ of such materials decrease sharply with the increase of frequency in the low-frequency region [51]. As a result, frequency-dependent variation of experimental values of ϵ' , ϵ'' , $\tan\delta$, M' , M'' and σ_{ac} parameters of D1, D2, D3, and D4 diodes may be ascribed to the specific distributions of interfacial states or to the inhomogeneous structure of the interface, to the their relaxation time and to the surface/dipole polarization at p-Si/ V_2O_5 interface.

Acknowledgements This research was supported by the Ataturk University Scientific Research Management Office, under Project number: PRJ2014/177. The authors would like to thank Ataturk University Scientific Research Management Office for their support.

Author Contributions EŞ: contributed to conceptualization, visualization, investigation, methodology and writing-review & editing. MS: contributed to conceptualization, visualization, investigation, methodology, writing-review & editing and supervision.

Funding Open access funding provided by the Scientific and Technological Research Council of Türkiye (TÜBİTAK). The authors did not receive support from any organization for the submitted work. The authors have no financial or proprietary interests in any material discussed in this article.

Data availability All data generated or analysed during this study are included in this article.

Declarations

Competing interests The authors declare that there is no conflict of interest.

Open Access This article is licensed under a Creative Commons Attribution 4.0 International License, which permits use, sharing, adaptation, distribution and reproduction in any medium or format, as long as you give appropriate credit to the original author(s) and the source, provide a link to the Creative Commons licence, and indicate if changes were made. The images or other third party material in this article are included in the article's Creative Commons licence, unless

indicated otherwise in a credit line to the material. If material is not included in the article's Creative Commons licence and your intended use is not permitted by statutory regulation or exceeds the permitted use, you will need to obtain permission directly from the copyright holder. To view a copy of this licence, visit <http://creativecommons.org/licenses/by/4.0/>.

References

1. G.C. Bond, S.F. Tahir, Vanadium oxide monolayer catalysts Preparation, characterization and catalytic activity. *Appl. Catal.* **71**, 6365 (1991)
2. G. Gu, M. Schmid, P.W. Chiu, M. Kozlov, E. Munoz, R.H. Baughman, V_2O_5 nanofibre sheet actuators. *Nat. Mater.* **2**, 3164 (2003)
3. A. Kumar, P. Singh, N. Kulkarni, D. Kaur, Structural and optical studies of nanocrystalline V_2O_5 thin films. *Thin Solid Films*. **516**, 912–918 (2008)
4. A.A. Akl, Thermal annealing effect on the crystallization and optical dispersion of sprayed V_2O_5 thin films. *J. Phys. Chem. Solids*. **71**, 223–229 (2010)
5. J.M. Li, K.-H. Chang, C.C. Hu, A novel vanadium oxide deposit for the cathode of asymmetric lithium-ion supercapacitors. *Electrochim. Commun.* **12**, 1800–1803 (2010)
6. F. Mattelaer, K. Geryl, G. Rampelberg, J. Dendooven, C. Detavernier, Amorphous and crystalline vanadium oxides as high-energy and high-power cathodes for three-dimensional thin-film lithium ion batteries. *ACS Appl. Mater. Interfaces*. **9**, 13121–13131 (2017)
7. S. Beke, A review of the growth of V_2O_5 films from 1885 to 2010. *Thin Solid Films*. **519**, 1761–1771 (2011)
8. A. George, A.D. Raj, Q. Yang, Structural characteristics and gas sensing response of V_2O_5 nanorod thinfilms deposited by hot filament CVD. *Sens. Actuators B* **378**, 133078–133088 (2023)
9. S. Beke, L. Korosi, S. Papp, L. Nánai, J.G. Kiss, V. Safarov, Nd YAG laser synthesis of nanostructural V_2O_5 from vanadium oxide sols: morphological and structural characterizations. *Appl. Surf. Sci.* **254**, 1363–1368 (2007)
10. N.K. Nandakumar, E.G. Seebauer, Low temperature chemical vapor deposition of nanocrystalline V_2O_5 thin films. *Thin Solid Films*. **519**, 3663–3668 (2011)
11. E. Shembel, R. Apostolova, V. Nagirny, D. Aurbach, B. Markovsky, Interrelation between structural and electrochemical properties of the cathode based on vanadium oxide for rechargeable batteries. *J. Power Sources*. **81–82**, 480–486 (1999)
12. K.H. Chang, C.C. Hu, $H_2V_3O_8$ single-crystal nanobelts: hydrothermal preparation and formation mechanism. *Acta Mater.* **55**, 6192–6197 (2007)
13. A. Bouzidi, N. Benramdane, A. Nakrela, C. Mathieu, B. Khelifa, R. Desfeux, A. Da Costa, First synthesis of vanadium oxide thin films by spray pyrolysis technique. *Mater. Sci. Engineering: B* **95**, 141–147 (2002)
14. R. Irani, S.M. Rozati, S. Beke, Structural and optical properties of nanostructural V_2O_5 thin films deposited by spray pyrolysis technique: Effect of the substrate temperature. *Mater. Chem. Phys.* **139**(2–3), 489–493 (2013)
15. E. Ayyildiz, Ç. Nuhoglu, A. Türüt, The determination of the interface-state density distribution from the capacitance-frequency measurements in Au/n-Si Schottky Barrier diodes. *J. Electron. Mater.* **31**, 119–123 (2002)
16. B. Kinaci, Dielectric properties of Au/SrTiO₃/p-Si structure obtained by RF Magnetron Sputtering in a wide frequency range. *Silicon*. **14**, 2717–2722 (2022)

17. H. Wang, H. Li, W. Cai, P. Zhang, S. Cao, Z. Chen, Z. Zang, Challenges and strategies relating to device function layers and their integration toward high-performance inorganic perovskite solar cells. *Nanoscale*. **12**, 14369–14404 (2020)
18. Z. Xu, Q. Zhuang, Y. Zhou, Y.S. Lu, X. Wang, W. Cai, Z. Zang, Functional layers of inverted flexible Perovskite Solar cells and Effective technologies for device commercialization, small struct., **4**: 2200338–2200377 (2023)
19. M. Yang, H. Wang, W. Cai, Z. Zang, Mixed-Halide Inorganic Perovskite Solar cells: opportunities and challenges. *Adv. Opt. Mater.* **11**(20), 2301052–2301087 (2023)
20. Y. Zhou, Z. Guo, S.M. Qaid, Z. Xu, Y. Zhou, Z. Zang, Strain Eng. Toward High-Performance Formamidinium-Based Perovskite Solar Cells Solar RRL. **7**(19), 2300438–2300464 (2023)
21. İ.M. Afandiyeva, İ. Dökme, Ş. Altindal, M.M. Bülbül, A. Tataroğlu, Frequency and voltage effects on the dielectric properties and electrical conductivity of Al–TiW–Pd₂Si/n-Si structures. *Microelectron. Eng.* **2**(85), 247–252 (2008)
22. S. Kar, S. Varma, Determination of silicon-silicon dioxide interface state properties from admittance measurements under illumination. *J. Appl. Phys.* **58**, 4256–4266 (1985)
23. D.K. Schroder, *Semiconductor Material, Device Characterization* (Wiley, Hoboken, NJ, 2006)
24. C.P. Symth, *Dielectric Behaviour and Structure* (McGraw-Hill, New York, 1955)
25. M.A. Kinch, *Semiconductors and Semimetals*, ed. by R.K. Willardson, A.C. Beer AC (Academic, New York, 1981)
26. E.H. Nicollian, J.R. Bews, *MOS Physics and Technology* Wiley, New York, 1982
27. E. Şenarslan, B. Güzeldir, M. Sağlam, Effects of surface passivation on capacitance-voltage and conductance-voltage characteristics of Al/p-type Si/Al and Al/V₂O₅/p-type Si/Al diodes. *J. Phys. Chem. Solids*. **146**, 109564–109576 (2020)
28. E. Şenarslan, B. Güzeldir, M. Saglam, Influence of anodic passivation on electrical characteristics of Al/p-Si/Al and Al/V₂O₅/p-Si/Al diodes. *J. Mater. Sci. Mater. Electron.* **28**, 7582–7592 (2017)
29. B. Şahin, H. Çetin, E. Ayvıldız, The effect of series resistance on capacitance–voltage characteristics of Schottky barrier diodes. *Solid State Commun.* **135**, 490–495 (2005)
30. A. Türüt, M. Sağlam, The determination of the density of Si-Metal interface states and excess capacitance caused by them. *Phys. B* **179**, 285–294 (1992)
31. M. Çakar, A. Türüt, The conductance and capacitance-frequency characteristics of the organic compound (pyronine-B)/p-Si structures. *Synth. Met.* **138**, 549–554 (2003)
32. E.H. Nicollian, A. Goetzberger, The Si-SiO₂–electrical properties as determined by the metal-insulator-silicon conductance technique. *Bell Syst. Tech. J.* **46**, 1055–1133 (1967)
33. C. Barret, A. Vapeille, Interfacial states spectrum of a metal-silicon junction. *Solid State Electron.* **19**, 73–75 (1976)
34. A. Tataroglu, Ş. Altindal, The interface states analysis of the MIS structure as a function of frequency. *Microelectron. Eng.* **85**, 542–547 (2008)
35. A. Baltakesmez, B. Güzeldir, M. Saglam, M. Biber, Interpretation of the I–V, C–V and G/ω-V characteristics of the Au/ZnS/n-GaAs/In structure depending on annealing temperature. *Phys. B: Phys. Condens. Matter.* **611**, 41280–41300 (2021)
36. S. Alptekin, A. Tataroglu, Ş. Altindal, Dielectric, modulus and conductivity studies of Au/PVP/n-Si (MPS) structure in the wide range of frequency and voltage at room temperature. *J. Mater. Sci. Mater. Electron.* **30**, 6853–6859 (2019)
37. Ö. Sevgili, Y. Azizian-Kalandaragh, Ş. Altindal, Frequency and voltage dependence of electrical and dielectric properties in metal-interfacial layer-semiconductor (MIS) type structures. *Phys. B: Phys. Condens. Matter.* **587**, 412122 (2020)
38. S.A. kayan, H.I. Unal, B. Sari, Electrical and dielectric characteristics of Al/Polyindole Schottky Barrier Diodes. II. Frequency dependence. *J. Appl. Polym. Sci.* **120**, 390–396 (2011)
39. A. Kumar, A. Kumar, K.K. Sharma, Investigation of Dielectric properties of Ni/n-TiO₂/p-Si/Al Heterojunction in wide range of temperature and voltage. *Int. J. Eng.* **35**, 698–705 (2022)
40. D. Rethwisch, G.W.D. Callister, *Materials Science and Engineering*, 2013
41. M. Singh, A. Dogra, R. Kumar, Effect of 50 MeV Li³⁺ ion irradiation on structural, dielectric and permeability studies of In₃S substituted Mg-Mn ferrite. *Nucl. Instr Meth B* **196**, 315–323 (2002)
42. N. Konofaos, E.K. Evangelou, X. Aslanoglou, M. Kokkoris, R. Vlastou, Dielectric properties of CVD grown SiON thin films on Si for MOS microelectronic devices. *Semicond. Sci. Technol.* **19**, 50–53 (2004)
43. D. Dayananda, P.L. Reddy, K. Deshmukh, Y.R. Kumar, M.K. Kesrala, T. Kar, K.K. Sadasivuni, S.K.K. Pasha, *MXene-based Flexible Polymer Composites as high Dielectric Constant Materials, Chap. 22, Mxenes and Their Composites, Synthesis, Properties and Potential Applications* (Micro and Nano Technologies, 2022), pp. 725–758
44. K. Deshmukh, M.B. Ahamed, R.R. Deshmukh, S.K.K. Pasha, P.R. Bhagat, K. Chidambaram, Biopolymer composites with High Dielectric performance: Interface Engineering. *Biopolymer Compos. Electron.*, 27–128 (2017)
45. Y. Badalia, Ş. Altindal, İ. Uslu, Dielectric properties, electrical modulus and current transport mechanisms of Au/ZnO/n-Si structures. *Progress Nat. Science: Mater. Int.* **28**, 325–331 (2018)
46. A. Chelkowski, *Dielectric Physics* (Elsevier, Amsterdam, 1980)
47. H. Tecimer, On the frequency–voltage dependent electrical and dielectric profiles of the Al/(Zn-PVA)/ p-Si structures. *J. Mater. Sci.: Mater. Electron.* **29**, 20141–20145 (2018)
48. K. Prabakar, S.K. Narayandass, D. Mangalaraj, Dielectric properties of Cd_{0.6}Zn_{0.4}Te thin films. *Phys. Status Solidi A* **199**, 507–514 (2003)
49. S. Demirezen, S.A. Yerişkin, Frequency and voltage-dependent dielectric spectroscopy characterization of Al/(Coumarin-PVA)/p-Si structures. *J. Mater. Sci.: Mater. Electron.* **32**, 25339–25349 (2021)
50. M.D. Migahed, M. Ishra, T. Fahmy, A. Barakat, Electric modulus and AC conductivity studies in conducting PPy composite films at low temperature. *J. Phys. Chem. Solids*. **65**, 1121–1125 (2004)
51. E. Yükseltürk, S. Bengi, The frequency dependent complex dielectric and electric modulus properties of Au/P3HT/n-Si (MPS) Schottky barrier diode (SBD). *J. Mater. Sci: Mater. Electron.* **34**, 1580–1593 (2023)
52. S.P. Szu, C.Y. Lin, AC impedance studies of copper doped silica glass. *Mater. Chem. Phys.* **82**, 295–300 (2003)
53. S. Tataroglu, M.M. Altindal, Bulbul, Temperature and frequency dependent electrical and dielectric properties of Al/SiO₂/p-Si (MOS) structure. *Microelectron. Eng.* **81**, 140–149 (2005)
54. B. Barış, Frequency dependent dielectric properties in Schottky diodes based on rubrene organic semiconductor. *Phys. E* **54**, 171–176 (2013)
55. I. Yucedag, S. Altindal, A. Tataroglu, On the profile of frequency dependent series resistance and dielectric constant in MIS structure. *Microelectron. Eng.* **84**, 180–186 (2007)
56. I. Karaduman Er, A.O. Cagirtekin, M. Artuc, S. Acar, Synthesis of Al/HfO₂/p-Si Schottky diodes and the investigation of their electrical and dielectric properties. *J. Mater. Sci: Mater. Electron.* **32**, 1677–1690 (2021)
57. I. Tunc, I. Dokme, S. Altindal, I. Uslu, Negative dielectric constant and electrical conductivity of Au/n-Si (111) Schottky Barrier Diodes with PVA/Ni,Zn Interfacial Layer. *J. Appl. Polym. Sci.* **122**, 265–272 (2011)

58. S.A. Yeriskin, E. Erbilen Tanrikulu, M. Ulusoy, Dielectric properties of MS diodes with ag:ZnO doped PVP interfacial layer depending on voltage and frequency. *Mater. Chem. Phys.* **303**, 127788 (2023)
59. Ö. Kaya, H. Vural, S. Tecimer, S. Demirezen, Altindal, Frequency and voltage dependence of dielectric properties and electric modulus in Au/PVC + TCNQ/p-Si structure at room temperature. *Curr. Appl. Phys.* **14**, 322–330 (2014)
60. H.H. Gullu, D.E. Yıldız, Capacitance, conductance, and dielectric characteristics of Al/TiO₂/Si diode. *J. Mater. Sci: Mater. Electron.* **32**, 13549–13567 (2021)

Publisher's Note Springer Nature remains neutral with regard to jurisdictional claims in published maps and institutional affiliations.